J|A|C|S
ARTICLES
Published on Web 08/25/2006

Automated Search for New Thermoelectric Materials: The Case of LiZnSb

Georg K. H. Madsen

Contribution from the Department of Chemistry, University of Aarhus, DK-8000 Århus C, Denmark

Received April 12, 2006; E-mail: georg@chem.au.dk

Abstract: An automated band structure calculation based on the inorganic crystal structure database and the augmented plane wave method for electronic structure calculations is presented. Using a rigid band approach and semiclassic Boltzmann theory the band structures are analyzed and a large number of compounds are screened for potential interesting thermoelectric properties. We thereby propose LiZnSb as a potential new thermoelectric material. The *k*-space structure of the lowest conduction band of LiZnSb is analyzed in detail, and excellent thermoelectric properties are expected for this material. Furthermore the lattice dynamics are calculated, and anisotropic lattice thermal conduction is predicted.

I. Introduction

The search for new thermoelectric materials is a quest to maximize the dimensionless figure of merit $zT = (\sigma T/\kappa)S^2$, where S is the Seebeck coefficient and σ and κ are the electronic and thermal conductivities, respectively. zT quantifies the performance of a thermoelectric, and one must therefore maximize the power factor $S^2\sigma$ and minimize κ. As S, σ, and κ are coupled and all depend strongly on the detailed electronic structure, carrier concentration, and crystal structure, the task of finding new compounds with large values of zT is extremely difficult.

One idea that seems to run as a red thread through much recent research on thermoelectrics, including the work on clathrates[1−9] and skutterudites,[10−12] is the concept of a "Phonon Glass Electron Crystal" (PGEC).[13] This concept is based on the assumption that low-frequency optical modes, due to loosely bound guest atoms inside a framework structure, will reduce the lattice thermal conductivity thereby enhancing the figure of merit. The PGEC concept was introduced by Slack,[13] who also established a correlation among the weighted mobility, the band gap, and the average electronegativity difference. Hereby a number of semiconductors were suggested as potentially interesting for thermoelectric applications.[13] While the idea of a PGEC has been highly influential, the use of the electronegativity difference for predicting suitable electronic properties has been less used.

A different approach to rationally improving the electronic properties of thermoelectrics is the analysis of band structure calculations using Boltzmann theory. This ab initio approach has been successful in rationalizing and predicting the optimal doping level of known compounds[5,11,14−17] but has seldomly been used to discover new interesting materials for thermoelectric applications. However, we do not see any reason why band structure calculations cannot be used to screen a large number of potential candidates. As the underlying basis of Boltzmann theory is well understood,[18] one usually understands when it should work. Briefly put, the crystal momentum should be well defined so that k is a good quantum number. In a crystal, this means that the mean distances between scatterers, and thereby the mean free path of the electron, should be large compared to the wavelength of the electron. Furthermore, the advance of computational power, methodology, and standardized software has made the calculation of band structures, even for a large system containing heavy atoms, quite straightforward. Finally, the calculation of a large number of structures is trivially parallel

(1) Nolas, G. S.; Cohn, J. L.; Slack, G. A.; Schujman, S. B. *Appl. Phys. Lett.* **1998**, *73*, 178−180.
(2) Cohn, J. L.; Nolas, G. S.; Fessatidis, V.; Metcalf, T. H.; Slack, G. A. *Phys. Rev. Lett.* **1999**, *82*, 779−782.
(3) Paschen, S.; Carrillo-Cabrera, W.; Bentien, A.; Tran, V. H.; Baenitz, M.; Grin, Y.; Steglich, F. *Phys. Rev. B* **2001**, *64*, 214404.
(4) Sales, B. C.; Chakoumakos, B. C.; Jin, R.; Thompson, J. R.; Mandrus, D. *Phys. Rev. B* **2001**, *63*, 245113.
(5) Madsen, G. K. H.; Schwarz, K.; Blaha, P.; Singh, D. J. *Phys. Rev. B* **2003**, *68*, 125212.
(6) Bentien, A.; Christensen, M.; Bryan, J. D.; Sanchez, A.; Paschen, S.; Steglich, F.; Stucky, G. D.; Iversen, B. B. *Phys. Rev. B* **2004**, *69*, 45107.
(7) Bentien, A.; Pacheco, V.; Paschen, S.; Grin, Y.; Steglich, F. *Phys. Rev. B* **2005**, *71*, 165206.
(8) Pacheco, V.; Bentien, A.; Carrillo-Cabrera, W.; Paschen, S.; Steglich, F.; Grin, Y. *Phys. Rev. B* **2005**, *71*, 165205.
(9) Madsen, G. K. H.; Santi, G. *Phys. Rev. B* **2005**, *72*, 220301.
(10) Sales, B. C.; Mandrus, D.; Williams, R. K. *Science* **1996**, *272*, 1325−1327.
(11) Singh, D. J.; Mazin, I. I. *Phys. Rev. B* **1997**, *56*, R1650−R1653.
(12) Keppens, V.; Mandrus, D.; Sales, B. C.; Chakoumakos, B. C.; Dai, P.; Coldea, R.; Maple, M. P.; Gajewski, D. A.; Freeman, E. J.; Bennington, S. *Nature* **1998**, *395*, 876−878.
(13) Slack, G. New materials and performance limits for thermoelectric cooling. In *CRC Handbook of Thermoelectrics*; Rowe, D. M., Ed.; CRC: Boca Raton, FL, 1995; pp 407−440.
(14) Møllnitz, L.; Blake, N. P.; Metiu, H. *J. Chem. Phys.* **2002**, *117*, 1302−1312.
(15) Scheidemantel, T. J.; Ambrosch-Draxl, C.; Thonhauser, T.; Badding, J. V.; Sofo, J. O. *Phys. Rev. B* **2003**, *68*, 125210.
(16) Thonhauser, T.; Scheidemantel, T. J.; Sofo, J. O. *Appl. Phys. Lett.* **2004**, *85*, 588−590.
(17) Bertini, L.; Gatti, C. *J. Chem. Phys.* **2004**, *121*, 8983−8989.
(18) Allen, P. B. Boltzmann theory and resistivity of metals. In *Quantum Theory of Real Materials*; Chelikowsky, J. R., Louie, S. G., Eds.; Klüwer: Boston, MA, 1996; pp 219−250.

10.1021/ja062526a CCC: $33.50 **© 2006 American Chemical Society**

and therefore well suited for present computer cluster architectures and future grid applications.

The aim of the present paper is two-fold: First, an "automated band structure method" and the parameters used will be described. The second part of the paper concerns the electronic structure and lattice dynamics of LiZnSb. LiZnSb has not previously been considered for thermoelectric applications, but we shall identify it as having a favorable band structure. Finally we will discuss the influence of some of the parameters and approximations used.

A. Rigid Band Approach to Conductivity. We have recently reviewed the calculation of transport tensors based on the Boltzmann equation and the rigid band approach (see ref 19 and references therein). Here we will introduce the concepts and the approximations used later in this paper.

The rigid band approach to conductivity is based on the transport distribution

$$\sigma_{\alpha\beta}(\epsilon) = \frac{1}{N}\Sigma_{i,\mathbf{k}}\,\sigma_{\alpha\beta}(i,\mathbf{k})\,\frac{\delta(\epsilon-\epsilon_{i,\mathbf{k}})}{\mathrm{d}\epsilon} \tag{1}$$

where the **k**-dependent transport tensor is given as

$$\sigma_{\alpha\beta}(i,\mathbf{k}) = \mathrm{e}^2\tau_{i,\mathbf{k}}\,v_\alpha(i,\mathbf{k})\,v_\beta(i,\mathbf{k}) \tag{2}$$

τ is the relaxation time, and $v_\alpha(i, \mathbf{k})$ is a component of the group velocities. The transport coefficients as a function of temperature, T, and chemical potential, μ, can be calculated by integrating the transport distribution

$$\sigma_{\alpha\beta}(T;\mu) = \frac{1}{\Omega}\int \sigma_{\alpha\beta}(\epsilon)\left[\frac{\partial f_\mu(T;\epsilon)}{\partial\epsilon}\right]\mathrm{d}\epsilon \tag{3}$$

$$\nu_{\alpha\beta}(T;\mu) = \frac{1}{eT\Omega}\int \sigma_{\alpha\beta}(\epsilon)\,(\epsilon-\mu)\left[\frac{\partial f_\mu(T;\epsilon)}{\partial\epsilon}\right]\mathrm{d}\epsilon \tag{4}$$

where f is the Fermi−Dirac distribution function. In this approach μ determines the number of carriers. The bands, and hence $\sigma(\epsilon)$, are left fixed (thus "the rigid band approach"). Therefore only one band structure calculation needs to be performed per compound.

In eqs 1−4 the relaxation time, τ, is unknown. In the present work it is treated as a constant. The validity of this approach has been tested earlier[15,20] and actually turns out to be a surprisingly good approximation even for systems with highly anisotropic crystal axes.[20] The Seebeck coefficient, $S = \sigma^{-1}\nu$, is then independent of τ and can thus be calculated on an absolute scale. The conductivity can however only be calculated with respect to the relaxation time, and τ must somehow be included as a parameter.

Apart from the power factor, one simple consideration can also be made when searching for the optimal zT: κ has both an electronic, κ_e, and a lattice, κ_l, component, and the ratio between T and κ_e is, to a good approximation, given by the Wiedemann−Franz relation: $\kappa_e = L_0\sigma T$. Inserting the Lorentz number, $L_0 = \pi^2/3(k_B/e)^2 = (156\ \mu\mathrm{V/K})^2$, zT is seen to be limited by the Seebeck coefficient

$$zT = \frac{S^2\sigma T}{\kappa_e+\kappa_l} = \frac{S^2}{L_0+\kappa_l/(\sigma T)} < \left(\frac{S}{156\ \mu\mathrm{V/K}}\right)^2 \tag{5}$$

For calculating zT also κ_l must be included, which will be discussed in sections III and IV.D.

II. Computational Method

Band structure calculations were performed using the L/APW+lo method[21] as implemented in the WIEN2k code.[22] The precision of the calculations are limited mainly by four factors: (i) the completeness of the basis set, (ii) the number of **k**-points used to sample the Brillouin zone (BZ), (iii) the exchange-correlation functional within density functional theory (DFT), and (iv) the precision of the experimental structure used. Factors (i) and (ii) can be improved systematically toward convergence, (iii) will be discussed below, and (iv) will be discussed both in section III and IV.D.

Regarding the basis set a plane wave cutoff defined by $\min(R_\alpha)$-$\max(k_n) = 5.6$ was found to be adequate. Also a correct description of relativistic effects is extremely important because several interesting thermoelectric materials contain very heavy atoms. In WIEN2k spin orbit coupling is included in a second variational step. We set the energy cutoff to 2.0 Ry for the second variational basis set and added $p_{1/2}$ local orbitals[23] to describe the strong spin orbit split p-contribution close to the Fermi level for the very heavy atoms (thallium to astatine). For the L/APW+lo method one must define an atomic sphere radius. This was done by a simple algorithm which set the sphere radius to 0.495× the shortest nearest neighbor distance. For the transition metal and rare earth atoms, the sphere size was increased by 8% and the max sphere size was set to 2.5 au. This algorithm has now been included in the WIEN2k code.[22]

Regarding the k-mesh, the number of k-points in the full BZ was set to 64×10^6 divided by the primitive unit cell volume (in au^3). For the self-consistent calculation a mesh 30 times less dense was used. For the calculations of the derivatives necessary for eq 2 we used a well tested smoothed Fourier interpolation to obtain an analytical expression of the bands.[19] The mesh was interpolated onto a mesh 5 times as dense as the original.

The exchange-correlation potential was calculated using both the Perdew−Burke−Ernzerhof (PBE)[24] and the Engel−Vosko (EV)[25] generalized gradient approximations (GGAs). The PBE-GGA[24] is the standard parameter-free GGA, while the EV-GGA has been designed by optimizing the exchange potential[25] rather than using E_{xc}. The reason for performing calculations using both GGAs is that standard GGA functionals are known to underestimate the band gap. Due to the $\partial f/\partial\epsilon$ factors in eqs 3 and 4, a correct band gap is important for an accurate prediction of thermoelectric properties, and the EV-GGA has been shown in several cases to give band gaps in good agreement with experiment.[26]

III. Searching the Database

The initial dataset was constructed by extracting all Sb containing compounds from before 1990 available in the Inorganic Crystal Structure Database.[27] This dataset consisted of 1630 structures. An initial screening removed all compounds

(19) Madsen, G. K. H.; Singh, D. J. *Comput. Phys. Commun.* **2006**, *175*, 67−71.
(20) Allen, P. B.; Pickett, W. E.; Krakauer, H. *Phys. Rev. B* **1988**, *37*, 7482−7490.
(21) Madsen, G. K. H.; Blaha, P.; Schwarz, K.; Sjöstedt, E.; Nordström, L. *Phys. Rev. B* **2001**, *64*, 195134.
(22) Blaha, P.; Schwarz, K.; Madsen, G. K. H.; Kvasnicka, D.; Luitz, J. *WIEN2k, An Augmented Plane Wave Plus Local Orbitals Program for Calculating Crystal Properties.* ISBN 3-9501031-1-2. Vienna University of Technology: Austria, 2001.
(23) Kuneš, J.; Novák, P.; Schmid, R.; Blaha, P.; Schwarz, K. *Phys. Rev. B* **2001**, *64*, 153102.
(24) Perdew, J. P.; Burke, K.; Ernzerhof, M. *Phys. Rev. Lett.* **1996**, *77*, 3865−3868.
(25) Engel, E.; Vosko, S. H. *Phys. Rev. B* **1993**, *47*, 13164−13174.
(26) Lykke, L.; Iversen, B. B.; Madsen, G. K. H. *Phys. Rev. B* **2006**, *73*, 195121.
(27) Inorganic Crystal Structure Database (ICSD). http://www.fiz-informationsdienste.de/en/DB/icsd/.

Table 1. Compounds Screened in This Study[a]

formula	space group	unit cell [Å]	angles [deg]	E_g [eV]	T [K]	n [e/u.c.]	zT
KZnSb	$P6_3/mmc$(194)	$a = 4.54(2)$	$\alpha = 90$	0.37 (PBE)	150	0.52/−0.08	0.14/0.14
12 161		$b = 4.54(2)$	$\beta = 90$	0.73 (EV)	300	0.51/−0.07	0.29/0.33
		$c = 10.50(2)$	$\gamma = 120$		600	0.43/−0.06	0.59/0.70
KZnSb	$P\bar{6}m2$(187)	$a = 4.535$	$\alpha = 90$	0.24 (PBE)	150	0.08/0.10	0.06/0.09
44 680		$b = 4.535$	$\beta = 90$	0.62 (EV)	300	0.08/0.11	0.20/0.27
		$c = 5.25$	$\gamma = 120$		600	−0.01/0.08	0.65/0.67
LiZnSb	$P6_3mc$(186)	$a = 4.431$	$\alpha = 90$	0.13 (PBE)	150	−0.03/−0.02	0.14/0.25
44 903		$b = 4.431$	$\beta = 90$	0.62 (EV)	300	−0.02/−0.01	0.58/0.89
42 064		$c = 7.157$	$\gamma = 120$		600	−0.01/−0.01	1.84/2.36
ZnSb	$Pbca$(61)	$a = 6.218$	$\alpha = 90$	0.13 (PBE)	150	−0.00/−0.01	0.07/0.06
76 937		$b = 7.741$	$\beta = 90$	0.45 (EV)	300	−0.01/−0.02	0.30/0.30
		$c = 8.115$	$\gamma = 90$		600	−0.02/−0.01	0.85/1.12
ZnSb	$Pbca$(61)	$a = 6.218$	$\alpha = 90$	0.05 (PBE)	150	−0.01/−0.01	0.06/0.08
43 653		$b = 7.741$	$\beta = 90$	0.43 (EV)	300	−0.01/−0.01	0.26/0.35
		$c = 8.115$	$\gamma = 90$		600	−0.03/−0.02	0.68/1.14
ZnSb	$Pbca$(61)	$a = 6.2016(8)$	$\alpha = 90$	0.07 (PBE)	150	−0.01/−0.01	0.07/0.08
43 265		$b = 7.7416(8)$	$\beta = 90$	0.43 (EV)	300	−0.01/−0.01	0.30/0.35
		$c = 8.0995(8)$	$\gamma = 90$		600	−0.02/−0.02	0.75/1.15
$ZnSnSb_2$	$I\bar{4}2d$(122)	$a = 6.273$	$\alpha = 90$	0.07 (PBE)	150	−0.01/−0.02	0.04/0.03
52 305		$b = 6.273$	$\beta = 90$	0.35 (EV)	300	−0.01/−0.02	0.18/0.15
		$c = 12.546$	$\gamma = 90$		600	−0.01/−0.03	0.64/0.52
$ZnSnSb_2$	$I\bar{4}2d$(122)	$a = 6.275$	$\alpha = 90$	0.04 (PBE)	150	−0.01/−0.02	0.05/0.03
42 669		$b = 6.275$	$\beta = 90$	0.20 (EV)	300	−0.01/−0.02	0.24/0.16
		$c = 12.55$	$\gamma = 90$		600	−0.01/−0.02	0.73/0.64
$BaZn_2Sb_2$	$Pnma$(62)	$a = 10.539(8)$	$\alpha = 90$	0.00 (PBE)	150	−0.03/−0.01	0.02/0.05
32 020		$b = 4.502(2)$	$\beta = 90$	0.20 (EV)	300	−0.05/−0.01	0.06/0.19
		$c = 11.639(8)$	$\gamma = 90$		600	0.23/−0.02	0.14/0.57
$TlZn_2Sb_2$	$I4$(79)	$a = 8.649(5)$	$\alpha = 90$	0.00 (PBE)	150	−1.55/−1.71	0.01/0.01
76 499		$b = 8.649$	$\beta = 90$	0.00 (EV)	300	−1.53/−1.69	0.02/0.05
		$c = 7.287(4)$	$\gamma = 90$		600	−1.49/−1.66	0.06/0.13
Hf_5ZnSb_3	$P6_3/mcm$(193)	$a = 8.514(3)$	$\alpha = 90$	0.00 (PBE)	150	−1.10/−1.07	0.01/0.01
42 913		$b = 8.514(3)$	$\beta = 90$	0.00 (EV)	300	−1.02/0.33	0.02/0.02
		$c = 5.747(3)$	$\gamma = 120$		600	−0.55/−0.20	0.05/0.06
$Ca_9Zn_4Sb_9$	$Pbam$(55)	$a = 21.92(2)$	$\alpha = 90$	0.00 (PBE)	150	−1.88/−1.56	0.00/0.01
52 787		$b = 12.50(1)$	$\beta = 90$	0.00 (EV)	300	−1.82/−1.60	0.01/0.02
		$c = 5.54(1)$	$\gamma = 90$		600	−1.45/−1.81	0.01/0.04
$SrZnSb_2$	$Pnma$(62)	$a = 23.05(5)$	$\alpha = 90$	0.00 (PBE)	150	−0.05/0.02	0.10/0.05
10 001		$b = 4.37(1)$	$\beta = 90$	0.00 (EV)	300	−0.06/0.05	0.21/0.14
		$c = 4.46(1)$	$\gamma = 90$		600	−0.11/−0.12	0.28/0.31
NaZnSb	$P4/nmmZ$(129)	$a = 4.44(2)$	$\alpha = 90$	0.00 (PBE)	150	−0.20/−0.27	0.04/0.02
12 154		$b = 4.44(2)$	$\beta = 90$	0.00 (EV)	300	−0.20/−0.26	0.11/0.07
		$c = 7.49(2)$	$\gamma = 90$		600	−0.18/−0.24	0.27/0.20
Zr_5Sb_3Zn	$P6_3/mcm$(193)	$a = 8.6074(7)$	$\alpha = 90$	0.00 (PBE)	150	−1.41/−1.47	0.01/0.02
57 595		$b = 8.6074$	$\beta = 90$	0.00 (EV)	300	−1.26/−1.34	0.04/0.03
		$c = 5.8362(8)$	$\gamma = 120$		600	−0.83/−0.71	0.06/0.06
$CaZn_2Sb_2$	$P\bar{3}m$(164)	$a = 4.441(1)$	$\alpha = 90$	0.00 (PBE)	150	−0.03/−0.03	0.03/0.03
12 150		$b = 4.441(1)$	$\beta = 90$	0.00 (EV)	300	−0.03/−0.04	0.09/0.10
		$c = 7.464(2)$	$\gamma = 120$		600	−0.04/−0.03	0.25/0.34
$SrZn_2Sb_2$	$P\bar{3}m$(164)	$a = 4.500(1)$	$\alpha = 90$	0.00 (PBE)	150	−0.05/−0.09	0.04/0.03
12 152		$b = 4.500(1)$	$\beta = 90$	0.00 (EV)	300	−0.05/−0.08	0.09/0.07
		$c = 7.716(2)$	$\gamma = 120$		600	−0.06/−0.08	0.21/0.22

[a] n corresponds to the carrier concentration giving the highest zT. For zT and n the first value is for the PBE calculation, and the second, for the EV. The zT values have been calculated using the band structure and the parameters: $\tau = 2 \times 10^{-14}$ s and $\kappa_l = 2$ W/mK. They are meant more as a brief index to identify compounds with favorable band structures than as quantitative predictions (see text for discussion). The structures have been labeled according to their chemical composition and their ICSD number.

which were (i) marked as wrong; (ii) contained disordered or partially occupied sites, which cannot be treated with the present band structure method; (iii) contained lanthanide atoms, because the highly localized 4*f* electrons need special consideration within DFT and are therefore unsuited for an automatic approach such as the present; or (iv) contained the highly electronegative elements N, O, F, and Cl atoms which would usually lead to short mean free paths. This reduced the dataset to 570 compounds, for which band structure calculations were performed and transport coefficients were extracted. Some compounds are reported in the literature as being air-sensitive and will therefore not be discussed further here. We will focus on

one interesting material, LiZnSb, which has not previously been considered for thermoelectric applications and has not been reported to be air-sensitive.

To illustrate the method and to set LiZnSb into context, we have chosen to present the compounds containing both Zn and Sb, Table 1. Of the ZnSb compounds considered, four are predicted to be narrow band gap semiconductors: KZnSb, LiZnSb, ZnSb, and $ZnSnSb_2$. The rest are predicted to be metals. As expected the EV potential increases the band gap significantly, but only in one case ($BaZn_2Sb_2$) does it open up a band gap.

We prefer to compare the compounds using an estimated zT, so κ_l and τ must be supplied as parameters. As a first estimate we chose $\kappa_l = 2$ W/(mK) and $\tau = 2 \times 10^{-14}$ s for Table 1. A $\kappa_l = 2$ W/(mK) is approximately 8 times the estimated minimal thermal conductivity,[13] and $\tau = 2 \times 10^{-14}$ s is approximately what has been found for the narrow band gap semiconductor Bi_2Te_3.[15] Thus, the parameters are not overly optimistic but are of course parameters, and their influence on the results will be considered in the final section.

All the narrow band gap semiconductors show reasonable thermoelectric properties, but only LiZnSb stands out at temperatures above 300 K (see next section). Here it is worth pointing out that one of the compounds, ZnSb, has been characterized experimentally.[28] zT has been found to increase with temperature up to around 0.6 at 250 K and to decrease at higher temperatures.[28] Quantitatively, the predicted zT at room temperatures is lower than the experimental, which underlines that the κ_l and τ parameters used could be on the conservative side. At higher temperatures the calculated zT is larger than experimental. This can be caused by τ decreasing with temperature, as would be expected if the scattering is dominated by an electron−phonon interaction or by impurity states being present in the band gap leading to an effectively lower band gap. Due to the unknown τ and κ_l, a quantitative agreement was not expected, and it should be underlined that the calculated values of zT are meant more as a brief index to identify compounds with favorable band structures than as quantitative predictions. However, it is important that the qualitative conclusion of the calculations, namely that ZnSb is expected to have reasonable, but not outstanding, thermoelectric properties, agrees with the experimental observation.

It should be pointed out that other previously known thermoelectric materials, such as the skutterudites[10−12,29] were also singled out. That the method was able to "find" already known thermoelectric materials we see as a proof-of-concept. Recently an alloy of Zn and Sb, Zn_4Sb_3, has been reported to have a $zT = 1.4$ at 400 °C.[28] The high-temperature structure is disordered and would therefore not be considered here. On the other hand, Zn_4Sb_3 has an ordered low temperature phase[30] which appears to be a narrow band gap semiconductor.[31] This illustrates both a shortcoming and an advantage of the present method: There is no way that an automized, high throughput method such as the present could have predicted that a disordered high-temperature structure of Zn_4Sb_3 would be that interesting. However, it is probable that the narrow band gap ordered structure[30,31] would have been singled out as an interesting compound (it has not been included here because the structure is so new that it has not yet been included in the databases).

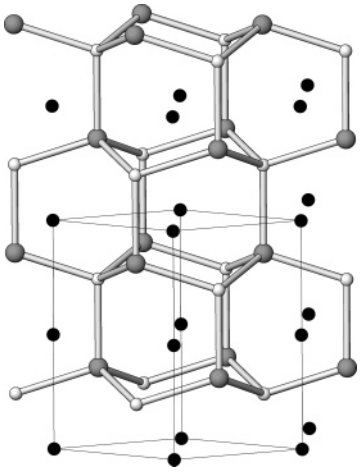

Figure 1. The structure of LiZnSb. Li: Black spheres. Zn: White spheres. Sb: Gray spheres.

Table 2. Bond Lengths in LiZnSb in Å

	experimental[32]	optimized
Li−Sb	2.89	3.02
Li−Zn	2.92	2.79
Zn−Sb	2.69	2.69
Zn−Sb	2.76	2.74

A further important point to be drawn from Table 1 is that the precision of the structure does not have a strong effect on the results. The structures of KZnSb and $ZnSnSb_2$ have been solved twice and ZnSb three times (KZnSb even in two different space groups). Still, the transport coefficients are in reasonable internal agreement.

IV. Intermetallic Lithium-Zinc-Antimonide

The structure of LiZnSb[32] is shown in Figure 1, and the bond distances are given in Table 2. Zn and Sb form an extended tetrahedrally coordinated framework with one bond slightly longer than the other three. Table 2 also gives the optimized distances. It can be seen that the Li position changes substantially. Usually one would expect DFT to give structural parameters in good agreement with experiment for a compound such as LiZnSb. As the structure determination is old,[32] it might have been difficult to precisely locate Li, when a strong scatterer such as Sb is also present. Fortunately, this does not seem to have a large influence on the predicted transport properties, which will be discussed Section IV.D. In the following the electronic structure of the experimental structure will be discussed.

A. Electronic Structure. LiZnSb belongs to the ternary transition metal pnictide class of Zintl compounds.[33] To a first approximation the electron count can be understood as: $Li^+(ZnSb)^-$, where each Li donates one electron to the ZnSb framework to fill the covalent bonding orbitals. Figure 2 shows the calculated density of states (DOS) of LiZnSb. The valence

(28) Snyder, G. J.; Christensen, M.; Nishibori, E.; Caillat, T.; Iversen, B. B. *Nat. Mater.* **2004**, *3*, 458−463.
(29) Slack, G. A.; Tsoukala, V. G. *J. Appl. Phys.* **1994**, *76*, 1665−1671.
(30) Nylén, J.; Andersson, M.; Lidin, S.; Häussermann, U. *J. Am. Chem. Soc.* **2004**, *126*, 16306−16307.
(31) Mikhaylushkin, A. S.; Nylén, J.; Häussermann, U. *Chem.—Eur. J.* **2005**, *11*, 4912−4920.
(32) Schroeder, G.; Schuster, H. *Z. Naturforsch., B: Anorg. Chem., Org. Chem.* **1975**, *30*, 978−979.
(33) Nesper, R. *Prog. Solid State Chem.* **1990**, *20*, 1−45.

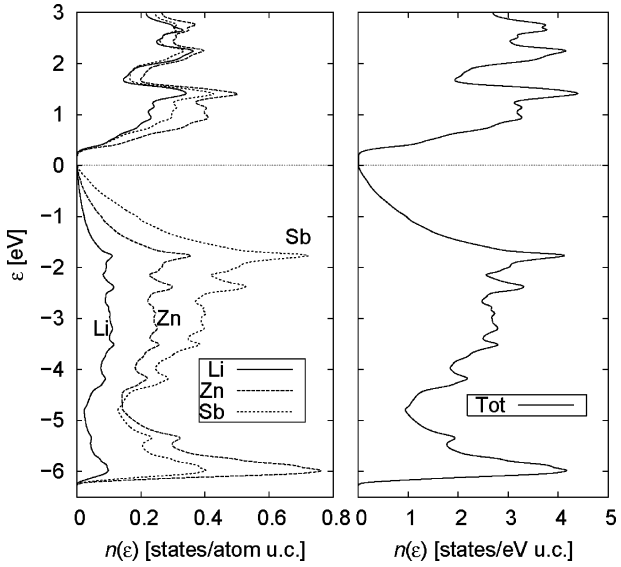

Figure 2. Calculated density of states for LiZnSb using the PBE-GGA.

states range over an energy interval of approximately 6 eV and are separated by a small energy gap of 0.13 eV (0.62 eV with the EV-GGA) from the conduction states. It is interesting to note that the DOS shows a strong covalency between all three atom types. This reflects how Li differs substantially from the heavier alkali metals in its tendency to form bonds with a high degree of covalency.[33]

The band structure of LiZnSb is given in Figure 3. The thin line marks the chemical potential that maximizes the power factor at 300 K (corresponding to a carrier concentration of 0.01 e/u.c.). At this carrier concentration it is clearly the lowest conduction band (LCB) which dominates the transport properties. It is seen that the LCB edge lies at the Γ-point and that a further electron pocket is found at the *L*-point at the zone boundary. Due to symmetry this pocket is 3-fold degenerate. Furthermore it is interesting to note an extra electron pocket just above the optimal chemical potential along the *L*−*LA* line (at $\mathbf{k} = 2\pi(^1/_2a^*, 0, 0.34c^*)$). These pockets are 6-fold degenerate and will thus contribute to a large change in the transport distribution at the optimal chemical potential and thereby to a large power factor.[15,19]

The plot of the total valence density shows the covalent bonding character of the Zn−Sb bonds (first box Figure 4). To understand the dispersion of the LCB, we have plotted the charge density of the LCB from the Γ, *L*, *LA* points and of the electron pocket along the *L*−*LA* line, Figure 4. At LCB-Γ the short Zn−Sb interaction is antibonding, while the longer one along the *c*-axis retains some bonding character. Furthermore, the interaction between the Zn and Sb of one neighboring tetrahedra, with a Zn−Sb distance of 4.40 Å, becomes bonding. At the *L* point all the Zn−Sb interactions in the tetrahedra are antibonding, but the bonding character of Zn to Sb in the next tetrahedra remains. Furthermore, there is a bonding interaction to the Li atoms and the nearest neighbor Zn and Sb. At the LCB energy minimum, along the *L*−*LA* line, the bonding to Li seems to be strong, with appreciable directional character of electron density at Zn and Sb toward Li. This directional character is not found at the *LA*-point, which also lies substantially higher in energy.

B. Transport Properties. The hexagonal symmetry of LiZnSb means that the conductivity tensors will be diagonal and that $\sigma_{xx} = \sigma_{yy} \neq \sigma_{zz}$. Figure 5 shows how the conductivity in LiZnSb is strongly anisotropic and that for the *n*-doped material σ_{xx} is as much as 5 times higher than σ_{zz} at 500 K. At

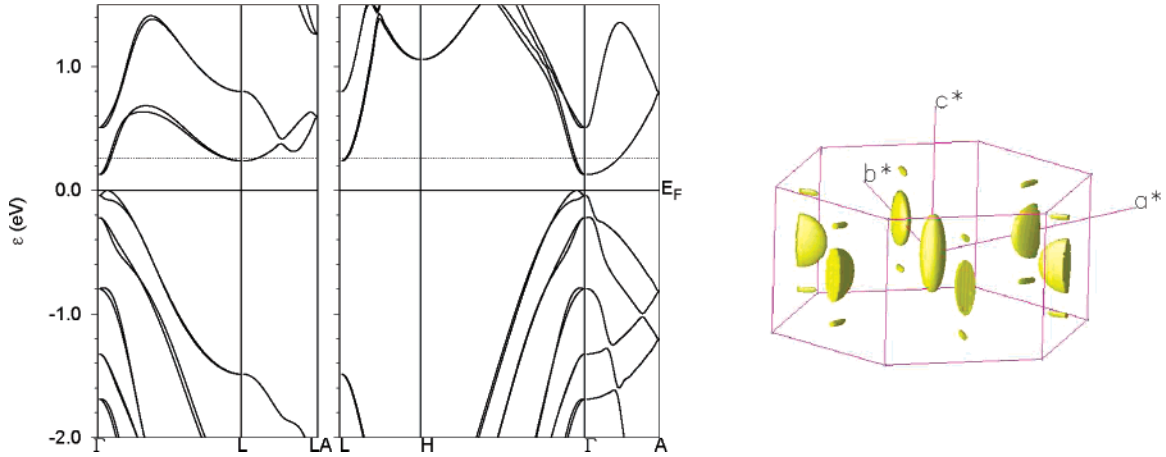

Figure 3. (a) Band structure of LiZnSb. The points are labeled according to the special points of the reciprocal *P*6*mm* space group. $L = (^1/_2, 0, 0)$, $LA = (^1/_2,0,^1/_2)$, $H = (^1/_3,^1/_3,0)$, and $A = (0, 0, ^1/_2)$ in the $2\pi(a^*, b^*, c^*)$ basis. (b) Constant energy surface of the LCB. The energy is set 0.05 eV above the optimal chemical potential marked in (a).

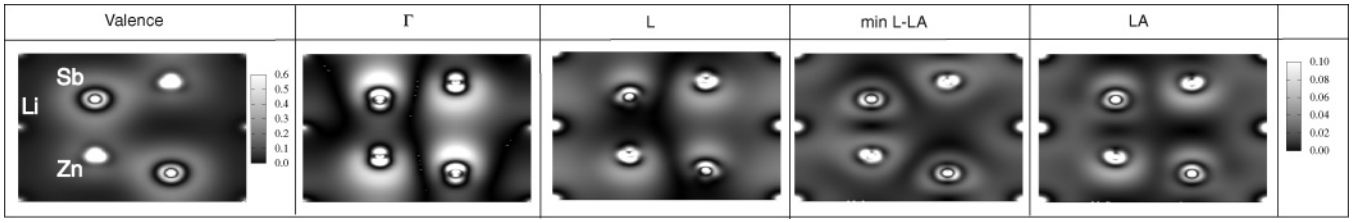

Figure 4. The valence charge density and the charge densities obtained by populating four selected points of the lowest conduction band. The plane shown is the −110 plane. The scale is in units of e/Å.[3] At the *LA*-point where the band is 4-fold degenerate the density has been divided by two.

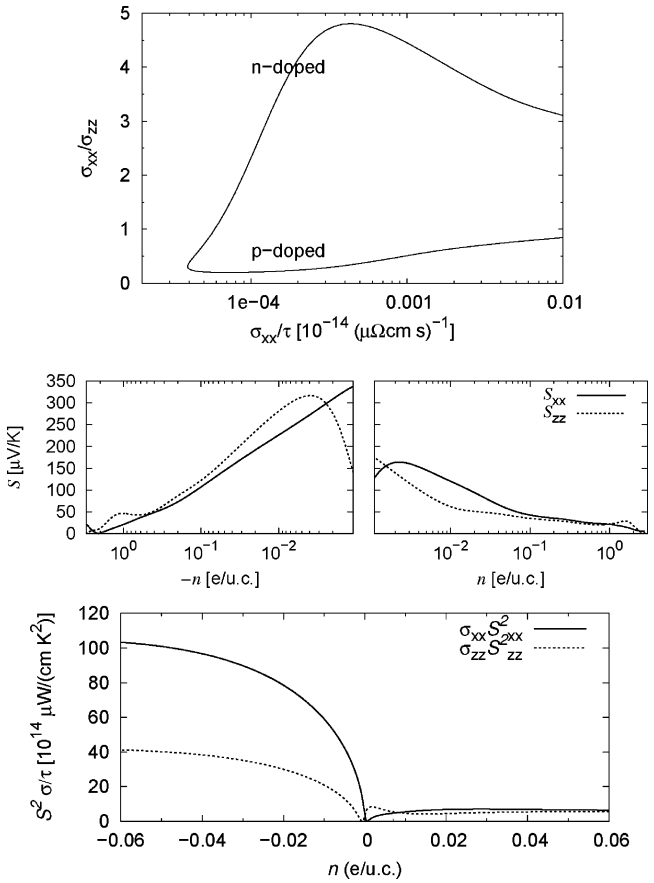

Figure 5. Transport properties calculated from the band structure of LiZnSb at 500 K. (a) Ratio of conductivity tensor components. (b) Seebeck coefficient as a function of carrier concentration. (c) $S^2\sigma/\tau$ as a function of carrier concentration. Note that τ has not been inserted as a parameter.

300 K it is up to 9 times higher, which is a much stronger anisotropy than is seen in, e.g., Bi_2Te_3 where the ratio is between 4 and 5.[15] Consequently S_{zz} is larger than S_{xx} for the *n*-doped material, but it is important to note that S_{xx} reaches values larger than 156 μV/K. This combination of large S_{xx} and large σ_{xx} results in the favorable thermoelectric properties, Figure 5c. The values reported in Table 1 are based on the traces of the transport tensors. Thus if the strong anisotropy in conductivity could be utilized, as done recently for the thermoelectric compound $CsBi_4Te_6$,[34] the thermoelectric properties would be even better in the *ab*-plane.

C. Calculated Lattice Dynamics. 1. Method. The phonon dispersion relations for LiZnSb were calculated within the harmonic approximation where all atomic potential terms above quadratic are ignored. The atomic positions were first relaxed to their equilibrium positions. For the phonon calculations a 2 × 2 × 1 super cell was set up. Due to the high symmetry this can be reduced to only 6 nonequivalent atomic displacements. A total of 12 calculations were done, displacing the atoms 0.02 Å both in positive and negative directions to compensate for possible small deviations from the equilibrium positions. The phonon frequencies were calculated with a modified version of the program PHON.[35]

2. Results. The calculated phonon density of states (PDOS) is shown in Figure 6. The PDOS can roughly be partitioned into three regions. The region between 0 and 10 meV is dominated by acoustic and two-body interactions. The region between 10 and 20 meV is dominated by three-body interactions. The region above 20 meV is dominated by Li motion that is little hybridized with the other atoms.

Figure 6 also depicts a weighted average of the squared group velocity of the modes[36] (the phonon velocity density of states (PVDOS)). v^2g enters the Boltzmann relaxation time approximation of thermal conductivity and can give a qualitative understanding of which modes contribute to the thermal conductivity. Not surprisingly, in the PVDOS the acoustic phonons have a higher weight. Furthermore, the modes between 10 and 15 meV have the main dispersion along the *c**-axis, and consequently $v^2_{zz}g$ is important. Also in the region above 20 meV two regions can be found with a much stronger dispersion along the *c**-axis. It is therefore expected that the lattice thermal conductivity will be strongly anisotropic with a lower κ_l in the *ab*-plane compared to the *c*-direction. Again, this could be an advantage if the anisotropy can be utilized, because the *ab*-plane also shows the best electronic properties.

D. Empirical Parameters and Precision of Estimate. Using the parameters $\tau = 2 \times 10^{-14}$ s and $\kappa_l = 2$ W/mK, a zT between 1.8 and 2.4 at 600 K was found for LiZnSb, Table 1. The estimated zT is dependent on the ratio between the two parameters κ_l and τ, eq 5. If τ is halved or κ is doubled the

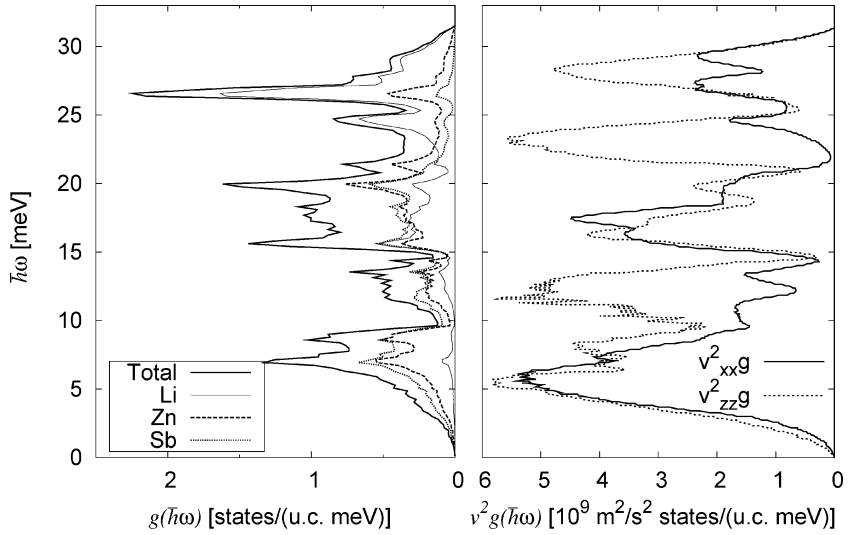

Figure 6. Calculated phonon and phonon velocity density of states for LiZnSb in the harmonic approximation.

Table 3. Influence of Parameters and Structure on the Estimated *zT* for LiZnSb at 600 K[a]

	κ_l/τ [10^{14} W/(Kms)]	*zT* (PBE)	*zT* (EV)
exp struct	1	1.84	2.36
	2	1.35	1.65
opt struct	1	1.89	2.28
	2	1.37	1.58

[a] $\kappa_l/\tau = 1 \times 10^{14}$ W/(Kms) corresponds to the parameters used in Table 1.

estimated max *zT* drops to between 1.4 and 1.7, Table 3, which is still reasonably high. A different source of uncertainty could be the experimental geometry used. In this respect it is interesting to note the difference in the Li position between the optimized structure and the experimental. It turns out that the transport properties change only little compared to the experimental structure, Table 3. This agrees well with the analysis in section III, where it was found that the differences between different structure determinations do not influence the results substantially.

This short analysis shows that a claim of $zT \approx 2$ for LiZnSb at 600 K is connected with a large uncertainty. However, it should also be pointed out that the κ_l and τ values used are not overly optimistic. So the uncertainty can also mean that *zT* for LiZnSb is underestimated.

V. Conclusion

We have reported an automated search procedure for new compounds for thermoelectric applications. Hereby, the Zintl compound LiZnSb has been suggested as a new thermoelectric material. We have reported a high *zT* value for LiZnSb, but it is important to realize that this value is based not only on the calculated band structure but also on estimated parameters and thus is associated with a large uncertainty. However, as our parameters were not overly optimistic, this uncertainty goes both ways, especially considering that the strong anisotropy of the transport properties might be utilized.

The electronic structure of LiZnSb was analyzed in detail, and the LCB was found to have a *k*-dependence leading to expectations of good thermoelectric performance. An appreciable covalent bonding to Li in the LCB contributes to the existence of electron pockets in the band structure leading to good thermoelectric properties.

For optimal performance of LiZnSb, a carrier concentration of approximately 0.01 e/u.c. is predicted, Table 1. One would expect it to be possible to introduce *n*-type carriers into the system by exchanging small amounts of Zn or Sb with small amounts of Ga or Te, respectively. The covalent radii are similar (1.25/1.26 Å for Zn/Ga and 1.40/1.36 Å for Sb/Te), and to a first approximation Zn and Sb form a covalently bonded network. It may be difficult to synthesize LiZnSb with the optimal carrier concentration, but a big advantage of the present approach is that it is based on known compounds with crystal structures that have been solved, so synthetic procedures are available.[32] We believe that as the analysis is improved and more structures with complicated crystal structures are tested, this approach to data mining will lead to several more interesting compounds.

Acknowledgment. A. Bentien and B. B. Iversen are thanked for useful discussions. The Carlsberg Foundation and the Danish Strategic Research Council are thanked for financial support. The computations were performed at the computer facilities of the Danish Center for Scientific Computing (DCSC), Odense, Denmark.

JA062526A

(34) Chung, D.-Y.; Hogan, T. P.; Rocci-Lane, M.; Brazis, P.; Ireland, J. R.; Kannewurf, C. R.; Bastea, M.; Uher, C.; Kanatzidis, M. G. *J. Am. Chem. Soc.* **2004**, *126*, 6414−6428.
(35) Alfé, D. http://chianti.geol.ucl.ac.uk/∼dario, 1998.
(36) Feldman, J. L.; Singh, D. J. *Phys. Rev. B* **1996**, *53*, 6273−6282.